AIAA JOURNAL
Vol. 31, No. 10, October 1993

Riemann Solvers for Perfect and Near-Perfect Gases

Jack Pike*
Chawston, Bedfordshire, MK44 3BH England, United Kingdom

The equations for the Riemann problem for a perfect gas or constant covolume equation of state are rewritten in terms of three similarity parameters and a weak dependence on the ratio of specific heats of the gases. These parameters are used to demonstrate the errors in the solutions of existing linearized Riemann solvers and to develop a new solver that has the simplicity of the linearized solvers but that is more accurate. Among nonlinear solvers, the two-expansion approximation is shown to be very accurate, except for flows involving strong shock waves. An equivalent two-shock approximation is developed that is very accurate for converging flows. It is combined with the two-expansion approximation to give an approximation that has a bounded error for all initial conditions. More accurate or exact solutions to the Riemann problem require iterative methods. Faster exact solvers are obtained by using the new approximations as starting values, by reformulating the iteration technique for faster convergence, and by using a "look-up" table to speed up part of the calculation. Average solution times are reduced to about two-thirds of the previously fastest method.

Nomenclature

a = speed of sound
b = covolume constant, Eq. (9)
c = velocity proportional to speed of sound, Eqs. (8) and (9)
du = velocity similarity parameter, Eq. (15)
E = error function, Eq. (33)
G = $2\gamma/(\gamma + 1)$, Eq. (3)
g = $(\gamma - 1)/(\gamma + 1)$, Eq. (2)
k = constant of iteration, Eq. (39)
P = nondimensional pressure, Eqs. (4) and (5)
p = static pressure
p_r = pressure ratio p_R/p_L, Eq. (13)
R = nondimensional density, Eqs. (10) and (11)
U = nondimensional velocity, Eqs. (6) and (7)
u = velocity
γ = ratio of specific heats
Δp = change in pressure
λ = similarity parameter, Eq. (14)
ρ = density

Subscripts

L = constant conditions left of discontinuity
R = constant conditions right of discontinuity

Superscripts

$*$ = conditions between outer waves
$'$ = differentiation with respect to P

I. Introduction

TO solve the Riemann problem,[1,2] the strengths of the waves emanating from an initial discontinuity in the fluid need to be determined. When the fluid is a perfect gas or a gas with a covolume equation of state, the wave system from the discontinuity has three waves, as shown in Fig. 1. The two outer waves are shock waves or expansions, and the inner wave is a contact discontinuity across which the pressure and velocity are continuous.[1,2] The initial conditions in the gases on either side of the discontinuity are taken to be constant and are specified by the pressure, velocity, and density of the gas together with the ratio of specific heats. When viscous and diffusive processes are neglected, the resulting wave system is self-similar in time, as indicated by the wave system shown in Fig. 1. The pressure and velocity are constant between the two outer waves, and the usual method of solution is to determine one of these by some iterative technique and then to find the other properties directly from this value. The inconvenience of an iterative solution has resulted in a number of approximate solutions of varying complexity, from simple linearized approximations[3-5] to more accurate nonlinear approximations,[6-8] such as the two-expansion approximation. The linearized approximations tend to be inaccurate for strong discontinuities; the two-expansion approximation is accurate for expansions and weak shock waves but is less accurate when the outer waves are strong shock waves. These approximate solutions can be used both directly and as starting values for the exact iterative solutions.

An important application of Riemann solvers is to computational fluid dynamics. For Godunov-type computation methods, the Riemann problem is solved in some manner at each cell boundary for each time step. An iterative solution is too slow to be used this extensively, and its use is confined to specialist methods such as the random choice method.[9] More generally, the faster approximate solutions of the Riemann problem are used, with different techniques being adopted for reducing the inaccuracy involved with strong shock waves. Toro[5] reverts to the exact iterative solution when some criteria are exceeded, but the sudden changes in the solution may prevent the convergence of steady flows. Roe[4] uses a linearization that is exact for a single shock wave.[10] This can still result

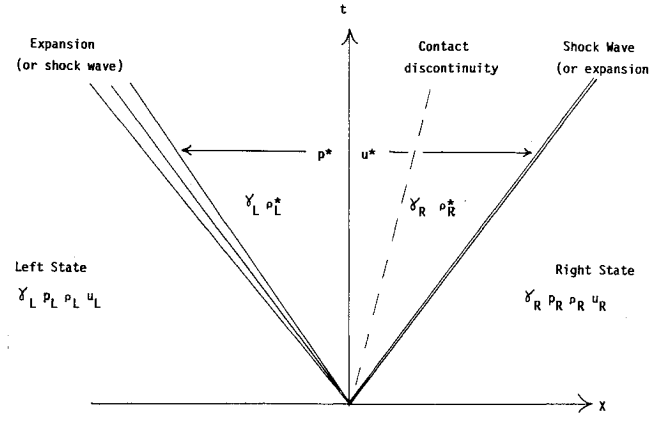

Fig. 1 Waves from a discontinuity separating constant flow states.

Received Nov. 5, 1992; revision received March 17, 1993; accepted for publication March 20, 1993.
*Holly Cottage. Member AIAA.

in large errors for shock interactions or shock reflections, however. The nonlinear approximation known as the Harten-Lax-Leer (HLL) method[6] involves estimating the velocities of the outer waves and then using conservation to establish the conditions between them. The original method neglected changes across the contact discontinuity and thus could become inaccurate when these changes were large. A similar but more complicated method that includes contact discontinuity has recently been published[7] and is shown to give good computational results. However, the accuracy still depends on the estimation of the wave speeds, including now the velocity of the flow between the outer waves for the velocity of the contact discontinuity.

The various errors that occur when using approximate Riemann solvers may be less significant in degrading the accuracy of the flow calculation than might be expected, because the flow often iterates in time toward the correct solution. However, for sensitive flows or flows where the details are important, it is difficult to be confident that using approximate Riemann solvers will not seriously affect the accuracy of the solution. Particular examples of flow calculations, or examples of the accuracy of the Riemann solver for particular initial conditions, can increase the confidence in the approximate solver, but to be able to confine the errors from the Riemann solver, one needs a systematic error analysis for the range of discontinuities of interest. There is then a need for a range of fast approximate Riemann solvers whose error characteristics are known for fast exact iterative procedures so that these may be more widely used.

II. Riemann Problem

The relationships between the velocity, density, and pressure for the constant regions between the waves have been derived in various forms from the Euler equations (representing conservation of mass, momentum, and energy) for both a perfect gas[3-8] and the constant covolume equation of state.[11] These complicated relationships, involving square roots when shock waves occur and fractional powers for expansions, are rewritten here in a more compact form that is less sensitive to differences in the ratio of specific heats across the initial discontinuity. That is, the velocity-pressure relationship for either outer wave is written for both a perfect gas and a covolume equation of state as

$$\begin{aligned} U(P,\gamma) &= (P-1)(1+g)^{1/2}/(P+g)^{1/2} && P \geq 1 \\ &= (P^G - 1)/G && P < 1 \end{aligned} \tag{1}$$

where U and P are the velocity and pressure ratios defined in Eqs. (4–7) and g and G are functions of γ given by

$$g = (\gamma - 1)/(\gamma + 1) \tag{2}$$

$$G = (\gamma - 1)/2\gamma \tag{3}$$

The ratios P and U are defined with respect to the flow states on either side of the initial discontinuity by

$$P_L = p^*/p_L \tag{4}$$

$$P_R = p^*/p_R \tag{5}$$

$$U_L = (u_L - u^*)/c_L \tag{6}$$

$$U_R = (u^* - u_R)/c_R \tag{7}$$

where the velocities c_L and c_R, used to nondimensionalize U_L and U_R in Eqs. (6) and (7), are defined differently for the different equations of state. For a perfect gas, c_L and c_R are the appropriate left or right speeds of sound over the ratio of specific heats; that is, dropping the suffixes,

$$c = a/\gamma \tag{8}$$

Similarly for the constant covolume equation of state

$$c = a(1 - b\rho)/\gamma \tag{9}$$

where $a = \sqrt{[\gamma p/\rho(1 - b\rho)]}$. The densities on either side of the contact discontinuity are expressed as density ratios

$$R_L = \rho_L^*/\rho_L \tag{10}$$

$$R_R = \rho_R^*/\rho_R \tag{11}$$

where the density ratio in terms of the pressure ratio is given for either the left or right values by

$$\begin{aligned} R &= (P+g)/(1+Pg) && P \geq 1 \\ &= P^{1-2G} && 0 \leq P \leq 1 \end{aligned} \tag{12}$$

The relationships shown for $P > 1$ (or $U > 0$) in Eqs. (1) and (12) are representative of shock conditions and those for $0 \leq P \leq 1$ of expansion or rarefaction conditions. When U is less than $-1/G$, representing a very divergent flow, vacuum conditions occur between the outer waves, and P and R are both zero.

The values of g and G defined in Eqs. (2) and (3) are both small for normal values of γ (i.e., $1 \leq \gamma \leq 1.67$). Thus the relationships as expressed earlier tend to be insensitive to changes in γ, and in particular Eq. (1) varies little with γ. This is illustrated in Fig. 2 where U is plotted as a function of P for γ values of 1 and 1.4. Other values of γ give similar curves.

The insensitivity of the problem as expressed in the form of Eq. (1) to the change in γ reduces the parameters defining the problem to three main similarity parameters, i.e.,

$$p_r = p_R/p_L \tag{13}$$

$$\lambda = c_R/(c_L + c_R) \tag{14}$$

$$du = (u_L - u_R)/(c_L + c_R) \tag{15}$$

and two subsidiary parameters γ_L and γ_R. In terms of these parameters, the Riemann solution requires P and U to satisfy

$$P_L = p_r P_R \tag{16}$$

$$(1 - \lambda)U_L + \lambda U_R = du \tag{17}$$

where $U(P, \gamma)$ is given by Eq. (1), or alternatively $P(U, \gamma)$ is given by the inverse form

$$\begin{aligned} P &= 1 + U\{U/2(1+g) + \sqrt{[1 + U^2/4(1+g)^2]}\} && U \geq 0 \\ &= (1 + GU)^{1/G} && -1/G \leq U \leq 0 \\ &= 0 && U \leq -1/G \end{aligned} \tag{18}$$

The solution to these equations in the form of Eqs. (1), (16), and (17) can be given a simple geometric interpretation, using the $U(P, \gamma)$ plot already shown in Fig. 2. In Fig. 3, only the $\gamma = 1.4$ curve is shown for simplicity. Consider some left wave of given strength, depicted by the point (P_L, U_L) on the $U(P, \gamma)$ curve in Fig. 3. Then the pressure ratio across the right wave can be obtained from Eq. (16) and the point (P_R, U_R) established on the curve, as shown. Inspection of Eq. (17) shows that, as λ varies from 0 to 1, the solution can be represented as a straight line joining (P_L, U_L) and (P_R, U_R) with du varying along the vertical axis from U_L to U_R. Thus this line represents the solution for all strengths of contact discontinuity, given the strengths of the two outer waves. If γ_L differs from γ_R, the points (P_L, U_L) and (P_R, U_R) will be on (slightly) different curves, but the straight line between them still represents all of the solutions for different initial density ratios.

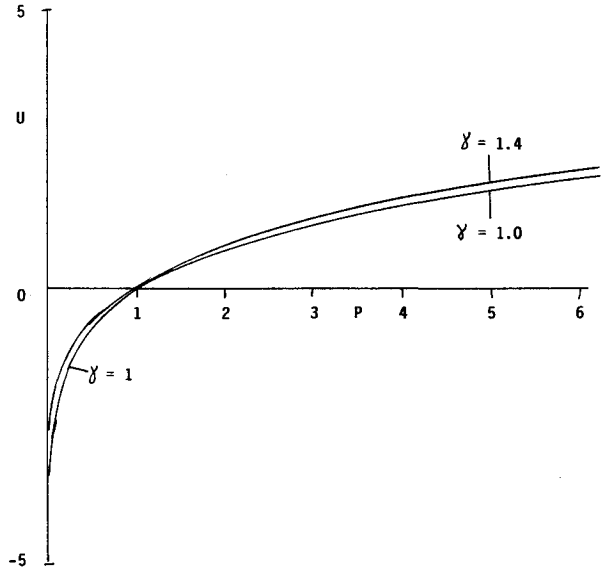

Fig. 2 Variation of $U(P, \gamma)$ with P for $\gamma = 1$ and 1.4.

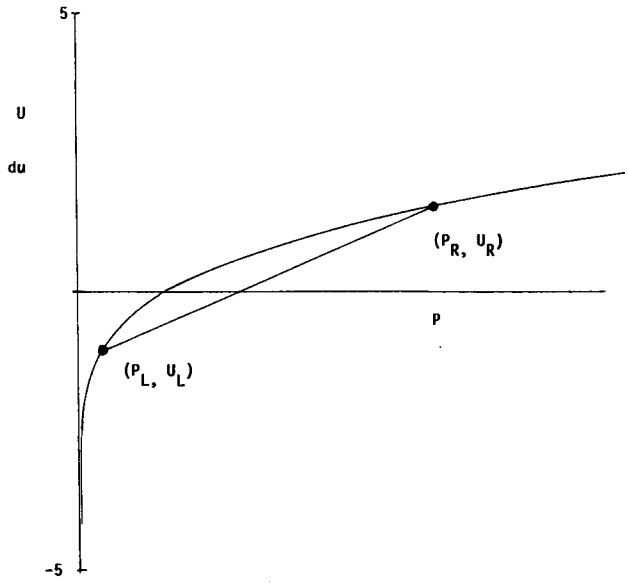

Fig. 3 Solution to the Riemann problem for given outer wave strength.

This representation can be used to illustrate certain properties of the solution. Assume first that $p_r < 1$, such that the left of the discontinuity is the high-pressure side; then P_R will lie to the right of P_L in Fig. 3, as shown. Then if du is positive, for the line between (P_L, U_L) and (P_R, U_R) to intersect the du value, P_R must be greater than 1 and the right wave will be a shock wave. Similarly, for if du is negative, the left wave will be an expansion. That is, if du is positive, the wave associated with the low-pressure side will be a shock wave, and if du is negative, the wave associated with the high-pressure side will be an expansion.

When P_L (or P_R) has a value of 1, then the appropriate outer wave has zero strength. The other wave is then a shock wave or expansion depending on whether du is positive or negative. More importantly, the complete solution is available immediately by making U_L (or U_R) zero in Eq. (17).

Another case for which an analytic closed solution exists is when p_r is unity and the points (P_L, U_L) and (P_R, U_R) coincide. The solution then requires the same du value for all values of λ, and the solution is given by $U_L = U_R = du$, with P obtained from Eq. (18). Note that this case includes the important symmetrical reflection condition used as a test case in the following section.

III. Approximate Riemann Solutions

Linearized Riemann solvers[3-5] are accurate for weak discontinuities but can exhibit large errors as the discontinuity becomes stronger. This can be demonstrated by comparing the approximate solutions with the exact solution for symmetrical conditions (i.e., $p_L = p_R$, $\rho_L = p_R$, $\gamma_L = \gamma_R$, and $u_L = -u_R$). Substitution of these conditions into Eqs. (16) and (17) gives $P_L = P_R$ and $U_L = U_R = du$. Thus the solution is the same as that shown in Fig. 2 with the U axis equal to du. The exact $\gamma = 1.4$ curve is replotted in Fig. 4. The Godunov[3] and Toro[5] expressions for p^* are given by

$$p^* = \frac{\rho_L a_L p_R + \rho_R a_R p_L + \rho_L \rho_R a_L a_R (u_L - u_R)}{\rho_L a_L + \rho_R a_R} \tag{19}$$

and

$$p^* = \tfrac{1}{2}(p_L + p_R) - \tfrac{1}{4}(\rho_L \rho_R)^{1/2}(a_L + a_R)(u_R - u_L) \tag{20}$$

respectively. These approximations are shown in Fig. 4 to give almost straight lines tangential to the exact curve at the point $P = 1$, resulting in large errors in the solution when P is not close to 1. Roe's approximation is shown in Fig. 4 to be more accurate, and it is also exact for a single shock wave. A much better approximation than these linear approximations is given by the two-expansion approximation, where the assumption is made that the left and right waves both can be represented by the expansion form of Eq. (1). Then from Eqs. (1) and (17) we have

$$du = (1 - \lambda)(P_L^{G_L} - 1)/G_L + \lambda(P_R^{G_R} - 1)/G_R \tag{21}$$

When γ_L is equal to γ_R, Eq. (21) can easily be inverted to give a direct expression for P. More generally, some approximation needs to be made to be able to invert the expression. We have seen in the previous section that the strongest expansion occurs on the high-pressure side of the discontinuity; thus an approximation that remains exact for a single expansion can be obtained by using the γ value for the high-pressure side throughout Eq. (21). This approximation is slightly simpler and more accurate (at least for $P \sim 1$) than the previous two-expansion approximation.[8] We have from Eq. (21) that

$$P_L = \left(\frac{1 + G\,du}{1 - \lambda + \lambda p_r^{-G}}\right)^{(1/G)} \tag{22}$$

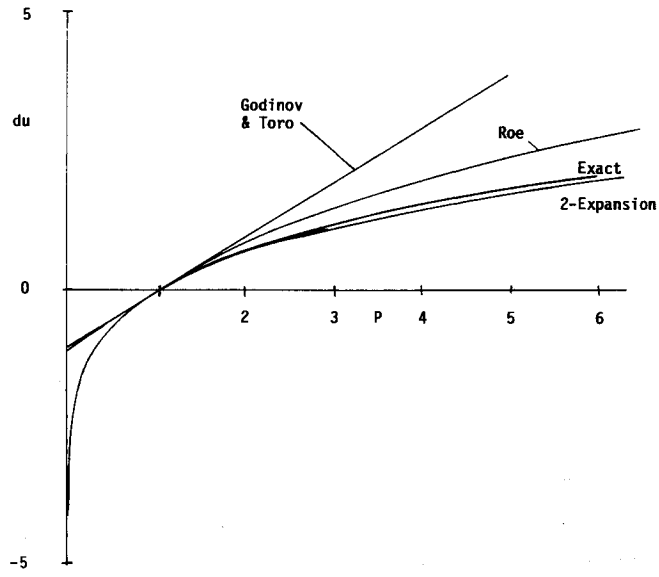

Fig. 4 Estimates of P for the symmetrical problem (i.e., $p_L = p_R$, $\rho_L = \rho_R$, $\gamma_L = \gamma_R$, $u_L = -u_R$).

where G defined in Eq. (3) uses the value of γ from the high-pressure side. It is shown in Fig. 4 that this approximation is close to the exact symmetrical curve at least for pressure ratios up to 6.

The disadvantages of the two-expansion approximation are the increasing errors for strong shock waves and the occurrence of fractional powers that are very time consuming to compute. A new alternative solution that is simple and accurate can be obtained by expanding Eq. (1) for P greater or less than 1 in terms of $P - 1$, i.e.,

$$U = \log P + \tfrac{1}{2}G(P-1)^2 + \mathcal{O}(P-1)^3 \tag{23}$$

Then, neglecting the latter small terms and substituting $\log P$ for U in Eq. (17) give the simple solution

$$U_L = \log P_L = du + \lambda \log p_r \tag{24}$$

with the densities given by Eq. (12). This approximation is almost indistinguishable from the exact curve in Fig. 4 but is less accurate for strong expansions than the two-expansion approximation. To remove the logarithmic function, Eq. (24) can be expanded to give

$$P_L = \frac{p_r + [1 - \lambda(1 - p_r)]^2}{1 + p_r}(1 + du/4)^4 \tag{25}$$

where the velocity and density are given by Eqs. (1) and (12). To avoid the fractional powers in Eqs. (1) and (12), it is sufficient to use the expression for $P > 1$ for all P. The approximation given by Eq. (25) for p^* is much more accurate than the linear approximations,[3-5] giving an estimate for the symmetrical case shown in Fig. 4 that is as good as the accuracy of the two-expansion approximation.

Although the example of Fig. 4 can show the inadequacy of an approximation, to demonstrate the accuracy over a wider range of conditions a systematic error analysis is needed. Such error analysis has been neglected in the past because of the number of parameters involved. The representation here, in terms of the three main parameters (p_r, λ, and du) and the two subsidiary parameters γ_L and γ_R, permits a more general error analysis, however. The value of p_r is always positive, and we can use the interchangeability of left and right states to restrict its range from 0 to 1 without loss of generality. The value of λ is restricted to the range from 0 to 1 by its definition. Thus for a given value of du and given γ values, we can plot the percentage error in p^* for all p_r and λ values. In Fig. 5a the error pattern for Eq. (25) is shown as a carpet plot for the range of p_r and λ values when $du = 0$ and $\gamma = 1.4$. We see that the error is larger at the intermediate values of λ and increases with decreasing p_r to a maximum value shown in Fig. 5a of about 30% when p_r is 0.1 (that is, for a pressure ratio of 10 across the initial discontinuity). As the pressure ratio increases, the percentage error in p^* becomes larger, a feature that is common to all of the approximations. The comparable plots for the linear solvers of Godunov, Toro, and Roe are shown in Figs. 5b and 5c with compressed vertical error scales. In Fig. 5b we see that, for du equal to 0, Godunov's Eq. (19) gives pressures that are too low at high-pressure ratios, with errors up to 40% for pressure ratios of 10. Although these errors are not very much larger than those of Eq. (25), this favorable comparison is confined to small values of du. At larger du values, the accuracy of Eq. (19) deteriorates rapidly, as was seen in Fig. 4 for the particular case of $p_r = 1$ and $\lambda = \frac{1}{2}$. The accuracy of Toro's approximation [Eq. (20)] is shown in Fig. 5c for du equal to 0. At this value of du, the accuracy of Toro's estimate is the same as the mean pressure estimate, and the accuracy of Roe's approximation is very similar. The error can be seen to vary significantly with the value of λ and to be larger than Eqs. (19) or (25) when du is zero.

For other values of du, the error patterns tend to be similar to those shown in Fig. 5, but the magnitude of the error

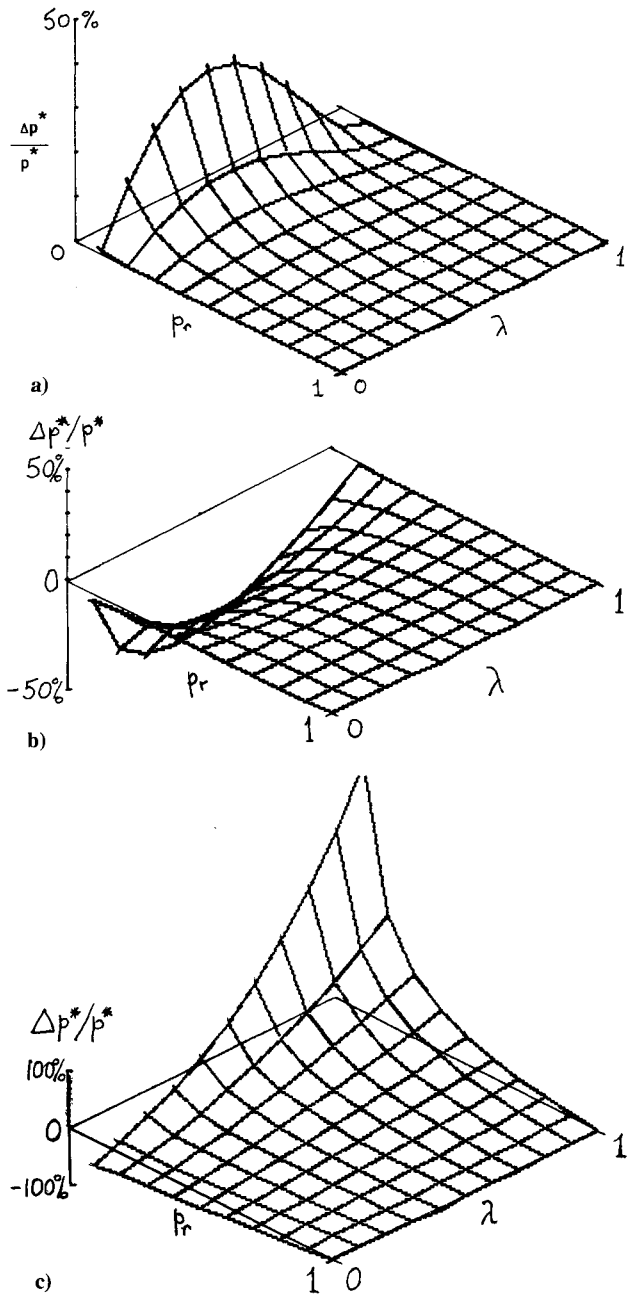

Fig. 5 Percentage error in p^* when $u_L = u_R$ and $\gamma = 1.4$: a) Eq. (25); b) Godunov,[3] Eq. (19); and c) Toro,[5] Eq. (20), and Roe.[4,10]

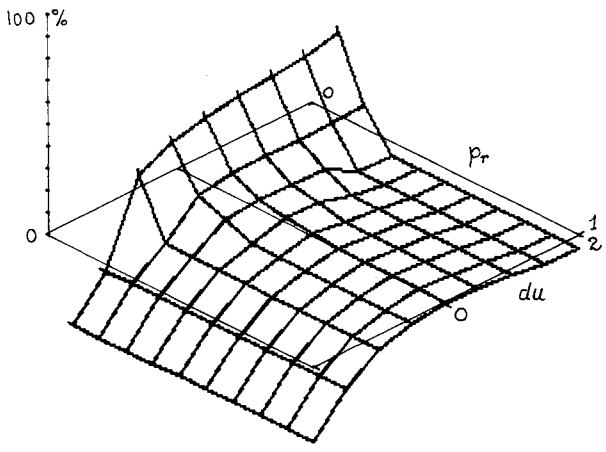

Fig. 6 Maximum percentage error in p^* for all λ, from Eq. (25).

changes. This is shown for the approximation of Eq. (25) in Fig. 6, where the maximum percentage error in p^* for all λ is plotted over a range of p_r and du. We see that for du values greater than about -1, the variation in the error is much the same as for du equal to 0. For du less than -1 (that is, for strong rarefaction conditions), the maximum error is larger over the complete range of p_r. However, because p^* is small for these conditions, the absolute error in p^* is small. Although a value of γ of 1.4 is used throughout Figs. 5 and 6, other values of γ between 1 and 5/3 only cause small changes in the errors.

These approximations have been compared using the percentage error in the pressure between the outer waves. The errors in the velocity and densities in this region are also important and need to be related to the pressure error. A relationship for the density errors can immediately be obtained from Eq. (12), but that for the velocity is less obvious because of the difference terms (such as $P-1$) that occur in Eq. (1). However, Eq. (1) can be approximated to the form of Eq. (24), when we can write

$$\frac{\Delta p^*}{p^*} = \frac{\Delta P}{P} = \Delta U = \frac{\Delta u^*}{c_L + c_R} \tag{26}$$

relating the absolute error in u^* to the percentage error in p^*, at least for P close to 1.

Comparison is made with the two-expansion approximation for the same conditions as Figs. 5 and 6 in Figs. 7 and 8. The accuracy of the two-expansion approximation for a wide range of conditions immediately becomes apparent. We see that this approximation is generally much more accurate than Eq. (25). The significant errors in the two-expansion approximation occur when du is positive such that strong shock waves occur. This error for strong shock waves is unfortunate, however, because the persistence of strong shock waves in the flow makes them a major feature of the flows in which they occur.

This deficiency of the two-expansion approximation prompts the development of an equivalent two-shock approximation, where, instead of treating shock waves as isentropic compressions as for the two-expansion approximation, expansion waves are treated as negative entropy shock waves. This assumption has been used as the basis of a previous approximation,[12] but the further assumptions made to obtain a solution give a complicated multicase approximation. In the two-shock wave case, Eq. (1) becomes

$$du = \frac{(1-\lambda)(P_L-1)(1+g_L)^{1/2}}{(P_L+g_L)^{1/2}} + \frac{\lambda(P_R-1)(1+g_R)^{1/2}}{(P_R+g_R)^{1/2}} \tag{27}$$

We have seen that the strongest shock wave occurs on the low-pressure side; thus, for $p_r<1$, changes to Eq. (27) to obtain a solution are confined to the first term on the right-hand side and when $p_r>1$ to the second term. This ensures

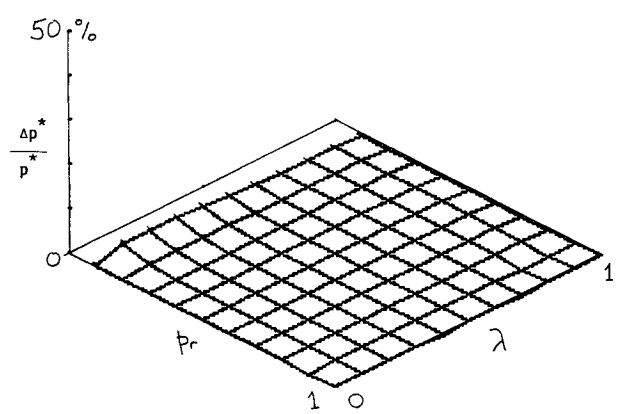

Fig. 7 Percentage error in p^* for the two-expansion approximation when $u_L = u_R$.

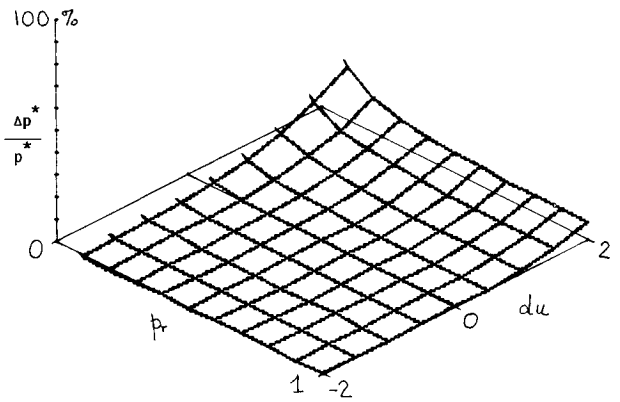

Fig. 8 Maximum percentage error in p^* for all λ from the two-expansion approximation.

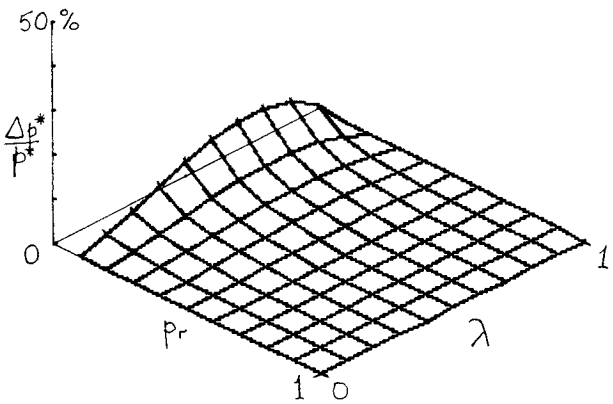

Fig. 9 Error in p^* for the two-shock approximation when $u_L = u_R$ and $\gamma = 1.4$.

that the approximation is exact for a single shock wave. Substituting for P_R from Eq. (16) gives

$$du = (1-\lambda)\frac{(P_L-1)(1+g_L)^{1/2}}{(P_L+g_L)^{1/2}} + \lambda\frac{(P_L-p_r)(1+g_R)^{1/2}}{p_r^{1/2}(P_L+p_r g_R)^{1/2}} \tag{28}$$

This equation can be solved exactly as a quadratic for P_L when g_L is equal to $p_r g_r$, which, incidentally, includes the symmetrical shock wave case of Fig. 4. Then by substituting $p_r g_R$ for g_L (or vice versa) in the denominator of Eq. (28), one obtains an approximation that is exact for the symmetrical shock wave case. That is,

$$P_L = c + 2d(d + \sqrt{c + d^2 + g_p}) \tag{29}$$

where

$$c = \frac{(1-\lambda)(1+g_L)^{1/2} + \lambda(1+g_R)^{1/2}p_r^{1/2}}{(1-\lambda)(1+g_L)^{1/2} + \lambda(1+g_R)^{1/2}/p_r^{1/2}} \tag{30}$$

$$d = \frac{du}{2(1-\lambda)(1+g_L)^{1/2} + 2\lambda(1+g_R)^{1/2}/p_r^{1/2}} \tag{31}$$

$$\begin{aligned} g_p &= g_R p_r \qquad p_r \le 1 \\ &= g_L \qquad p_r > 1 \end{aligned} \tag{32}$$

This is algebraically more complicated than the two-expansion approximation, but it does not contain fractional powers and is quicker to compute. It can be simplified slightly by relaxing the requirement that it is exact for very strong shock waves by taking the γ value to be that from the low-pressure side of the discontinuity throughout. Its accuracy for $du = 0$ and $\gamma = 1.4$ is shown in Fig. 9. The maximum error for all λ over the range $-2 < du < 2$ is shown in Fig. 10. We see that the error pattern

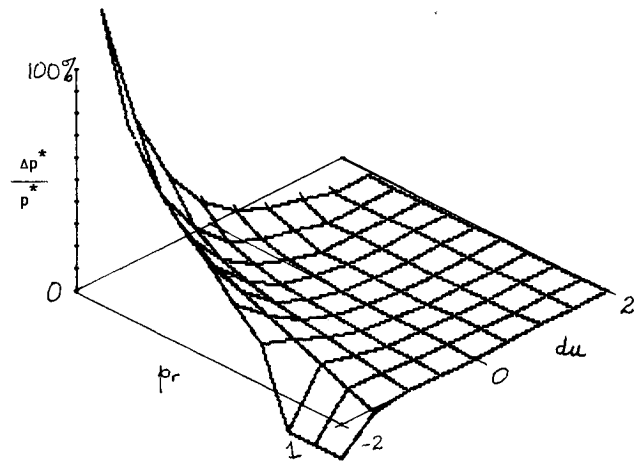

Fig. 10 Maximum percentage error in p^* for all λ, from the two-shock approximation.

is complementary to that of the two-expansion expression in that the accuracy improves as du becomes larger.

The complementary nature of the error pattern can be used to advantage by combining the two-shock and two-expansion approximations, that is, by using the two-shock approximation for positive du and the two-expansion approximation otherwise to give the two-expansion, two-shock (TETS) approximation. This approximation has the property of being exact for single or symmetrical outer waves or, more generally, for any two shock waves where $p_L g_L = p_R g_R$ or any two expansions where $\gamma_L = \gamma_R$. The maximum error for constant γ occurs when du is 0 and is shown in Fig. 9 for $\gamma = 1.4$. An upper limit on the percentage p^* error is given approximately by the initial pressure ratio across the discontinuity expressed as a percentage [i.e., p_r% or $(1/p_r)$% for $p_r < 1$], such that a pressure ratio of 10 will have a maximum error (overestimate) in p^* of about 10%. This error bound can be further reduced for constant γ, by using a nonzero value of du for the bound between the two-expansion and two-shock approximations (e.g., a du boundary at $2\gamma - 2.2$ reduces the maximum error to about 5% for $p_r > 0.1$). The accuracy of the TETS solution, or the simplicity of Eq. (25), make them good candidates for starting the fast iterative solution considered in the next section.

IV. Exact Iterative Solutions

Solutions of the Riemann problem to any specified accuracy can be obtained using an iterative solution, but the process may be slow. The total calculation time depends on the calculation time and accuracy of the initial estimate, plus the calculation time of each iteration times the number of iterations. The calculation time has been reduced by successive authors, usually using an iteration technique based on p^*, until total times of about one-third of the original Godunov method are available.[8] The fastest solutions are due to Gottlieb and Groth[8] and depend on three developments. First, the iteration variable used is u^*, which simplifies the algebra. Second, the starting estimate for u^* is obtained from the two-expansion approximation, which, although slower to compute, is much more accurate than linear approximations. Third, a simple first-order iteration technique is used, which, although requiring more iterations than higher order techniques, gains overall because of the quicker calculation time. Clearly, some further advantage may be gained by using the simpler or more accurate starting approximations of the previous section. However, for greater reductions in the mean solution time, it is necessary to improve the iteration also. Here we develop a near second-order iterative method with faster convergence, but whose calculation time is close to the first-order method. We also exploit the representation of the problem in the form of Eq. (1) to develop a fast "look-up" table for $U(P, \gamma)$ that reduces the calculation time.

An error function for the iterative process is defined from Eq. (17) to be

$$E = du - (1 - \lambda)U_L - \lambda U_R \tag{33}$$

Expanding E as a Taylor series in terms of p^* and rearranging give

$$\Delta P_L = \frac{E}{E'} - \tfrac{1}{2}(\Delta P_L)^2 \frac{E''}{E'} + \mathcal{O}(\Delta P_L)^3 \tag{34}$$

where E' is dE/dP_L. This can be rewritten in the form

$$\frac{\Delta P_L}{P_L} = \frac{E}{P_L E'} - \frac{1}{2}\left(\frac{E}{P_L E'}\right)^2 \frac{P_L^2 E''}{P_L E'} + \mathcal{O}(P_L)^3 \tag{35}$$

From Eq. (33) the term $P_L^2 E''/P_L E'$ is given by

$$\frac{P_L^2 E''}{P_L E'} = \frac{(1 - \lambda)(P^2 U'')_L + \lambda (P^2 U'')_R}{(1 - \lambda)(PU')_L + \lambda (PU')_R} \tag{36}$$

where $(PU')_R$ is $P_R dU_R/dP_R$. From Eq. (1), PU' and P^2U'' can be derived to be

$$\begin{aligned} PU' &= \frac{P}{2}\left[\left(\frac{P+g}{1+g}\right)^{-1/2} + \left(\frac{P+g}{1+g}\right)^{-3/2}\right] && P \geq 1 \\ &= P^G = 1 + GU && P < 1 \end{aligned} \tag{37}$$

and

$$\begin{aligned} P^2U'' &= -G\frac{P^2}{4}\left[\left(\frac{P+g}{1+g}\right)^{-3/2} + 3\left(\frac{P+g}{1+g}\right)^{-5/2}\right] && P \geq 1 \\ &= (G-1)P^G = (G-1)PU' && P < 1 \end{aligned} \tag{38}$$

Thus P^2U''/PU' varies from $-(\gamma+1)/2\gamma$ for $P < 1$ to $-\frac{1}{2}$ as P becomes large. Assuming a constant representative value k for this function between these two values, we can write Eq. (35) as

$$\frac{\Delta P_L}{P_L} = -\frac{E}{P_L E'} - \frac{k}{2}\left(\frac{E}{P_L E'}\right)^2 \tag{39}$$

and an iterative procedure for P_L becomes

$$P_L^{(n+1)} = P_L^{(n)}\left[1 - \frac{E}{P_L E'} - \frac{k}{2}\left(\frac{E}{P_L E'}\right)^2\right] \tag{40}$$

If the value of k is chosen such that the neglected part of the term of order $(E/P_L E')^2$ has a coefficient that is always less than 1, then when $P_L^{(n+1)}$ differs from $P_L^{(n)}$ by some small quantity, the error in $P_L^{(n+1)}$ will be less than this quantity squared, giving rapid convergence. The simplest value of k to meet this requirement is k equal to 0, but even faster convergence can be obtained by using a value of k between $-\frac{1}{2}$ and $-(\gamma+1)/2\gamma$. To ensure convergence for all starting conditions, we use $-\frac{1}{2}$, when Eq. (40) becomes simply

$$P_L^{(n+1)} = P_L^{(n)}\left(1 - \frac{E}{2P_L E'}\right)^2 \tag{41}$$

where

$$\frac{E}{P_L E'} = \frac{du - (1 - \lambda)U_L - \lambda U_R}{-(1 - \lambda)(PU')_L - \lambda (PU')_R} \tag{42}$$

The number of iterations needed depends on the required accuracy and the rate of convergence. As an example we consider the convergence patterns for an initial discontinuity with a pressure ratio of 10 and no change in the other variables (i.e., $p_r = 0.1$, $du = 0$, $\lambda = \frac{1}{2}$, and $\gamma = 1.4$). In Fig. 11 the

error in the pressure [as $\log_{10}(\Delta p^*/p^*)$] is plotted against the number of iterations for various starting approximations and two values of k. The starting pressures used are the mean pressure (equivalent to Toro's approximation when $du = 0$), the pressure from Eq. (25), and the pressure from the TETS approximation. The accuracy of these starting values is shown by the starting points on the vertical error axis representing the zero iteration line. The convergence of the first-order iteration method ($k = 0$) from each of these starting values is shown by the dotted lines. We see that the error in this case reduces approximately as $(\Delta p^*)^2$. Starting with Eq. (25) rather than the mean pressure as an initial estimate reduces the number of iterations by about one. Starting with the TETS approximation reduces the number of iterations needed by about two. There is a balance between the extra calculation time for the more accurate initial estimates and the number of iterations needed. The solid lines on Fig. 11 show the convergence of the near second-order method of Eq. (41) with k equal to $-\frac{1}{2}$. We see that convergence is faster, such that starting from the mean pressure estimate, two iterations with $k = -\frac{1}{2}$ achieve nearly the same level of convergence as three iterations with $k = 0$. For the more accurate starting conditions, the improvement is less. To assess the relative calculation times of the various options, we consider a range of initial conditions. These are given by $\gamma = 1.4$, $p_r = 0.1(0.01)1$, $du = -1(0.2)1$, and $\lambda = 0.05(0.1)0.95$ representing 10,010 Riemann problems that are solved to within $\mathcal{O}(10^{-6})$ in p^* (or u^* where appropriate). The mean times and the number of iterations are shown in Table 1, where each row shows a different starting estimate and each column a different iteration technique. The mean number of iterations per solution is shown on the left of each column, and the solution time in Fortran relative to the fastest solution technique is shown on the right. The relative calculation times of the starting estimates without any iterations are shown for reference in the first column. Of the five different starting estimates shown, we see that the simple algebraic expressions of Godunov, Toro, and Eq. (25) for p^* are about twice as fast to compute as the TETS estimate for p^* or the two-expansion estimate for u^*. The calculation times of the TETS and two-expansion estimation are dominated by the calculation of the fractional powers and can approach half the total iteration time. Note that, although the two-expansion estimate for u^* only uses one fractional power for each expansion calculation, whereas the estimate of p^* needs two, the TETS starting estimate uses on average only half the number of expansion calculations, giving similar calculation times for the two starting estimates. When these starting estimates are combined with a first-order iteration technique, the mean number of iterations and the average time to converge are shown in the second column. We see that the linear estimates of the first two rows require about four iterations to converge and require times that are over twice the minimum convergence time. The improved accuracy of Eq. (25) reduces the number of iterations required to about two and the time for convergence to about one-third greater than the minimum time. Using the accurate TETS starting estimation, the mean number of iterations required falls to 1.37 per solution, but the increased time for the starting estimate calculation restricts the reduction in the calculation time. These values need to be compared with the method of Ref. 8, which uses the two-expansion estimate of u^* to start the iteration. We see that the number of iterations needed is two on average, giving a mean solution time 47% above the minimum and significantly above the best first-order accurate iteration time. The third column shows the iterations and times for the near second-order method of Eq. (41). We see that when several iterations are required, as for the Godunov and Toro starting estimates, then using the second-order iteration method of Eq. (41) can significantly reduce the number of iterations and the solution time. However, when the number of iterations is two or less, the reduction is small. Thus the advantages of the faster second-order iteration technique are confined mainly to Riemann solutions with stronger shock waves or expansions or to more complicated Riemann problems that require larger numbers of iterations (for example, when the starting conditions depend on the Riemann solution).

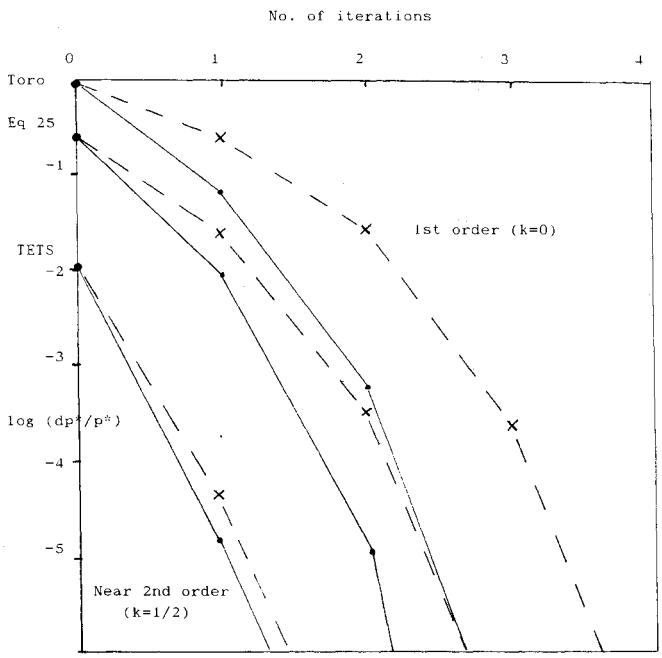

Fig. 11 Convergence of iterations from various starting estimates for case $p_R = 0.1$, $du = 0$, $\lambda = 0.5$, and $\gamma = 1.4$.

Table 1 Mean iteration and solution times for Riemann solvers

Starting estimate	Starting calculation		First-order iteration		Second-order iteration		Second-order and look up	
	Iters.	Time	Iters.	Time	Iters.	Time	Iters.	Time
Godunov	0	0.17	3.4	1.95	3.1	1.85	3.1	1.50
Toro	0	0.20	4.3	2.75	3.4	2.16	3.4	1.80
Eq. (45)	0	0.20	2.1	1.32	2.0	1.28	2.0	1.02
TETS	0	0.41	1.37	1.15	1.36	1.16	1.36	1.00
$2E(u^*)$	0	0.35	2.00	1.47	←Ref. 8			

The final column shows the iteration times when the expression of Eq. (1) is obtained from linear interpolation of a table of values. For accuracies of $\mathcal{O}(10^{-6})$, approximately 1000 values of U are required using linear interpolation when the value of γ is constant and several thousand values for a range of γ. Using precalculated values for U is about four times quicker than calculating the value, but when the other parts of the iteration are included, the improvement is more modest, reducing the calculation time by about one-quarter using Eq. (25) starting conditions and about one-sixth for TETS starting conditions. The final calculation times for these two starting conditions are very close, and the selection between them will depend on the particular application. In general, however, using Eq. (25) as the starting value is the more adaptable, in that most of the time is spent iterating. In either case the mean computation time is about two-thirds of that for the method of Ref. 8.

V. Conclusions

The equations representing the Riemann problem for a perfect gas or constant covolume equation of state are rewritten in terms of three similarity parameters plus a weak dependence on the ratio of specific heats of the gases on either side of the initial discontinuity. A systematic error analysis of some existing Riemann solvers shows that the linearized solvers can give large errors for strong disturbances and that the nonlinear

two-expansion approximation is very accurate except for converging flows that produce strong shock waves. Two new approximations are developed. The first has the simplicity of the linearized approximations but is much more accurate. The second is a two-shock approximation, which is accurate for strong shock wave solutions and exact for single and reflected shock waves but is less accurate for strong expansions. The two-shock and two-expansion approximations are combined to give the TETS approximation that has an overall error bound for the pressure for any starting conditions. The error bound of this approximation for constant γ can be simply expressed as the error in the pressure between the outer waves (p^*) quoted as a percentage that is less than the ratio of the pressures across the initial discontinuity.

The rewritten governing equations and the new approximate solutions are used to find faster exact iterative solvers for the Riemann problem. Three improvements are made, which can be used separately or in combination to improve the solution times. First, the number of iterations required to converge to the correct solution is reduced by using the more accurate initial conditions from the new approximations. Second, the iterative procedure is made more convergent without increasing the iteration time by including an estimate for the second derivative term. Third, the rewritten equations permit a look-up table to be used to reduce the amount of calculation for each iteration. The new solver is tested over a wide range of initial conditions and is found on average to take only about two-thirds of the calculation time of the previous fastest solver.

Although these techniques are developed and validated here for perfect gases (with an extension to the constant covolume equation of state), it is envisaged that some or all of the techniques might be applied to more general equations of state with the potential for greater savings in their usually longer solution times.

References

[1]Smoller, J., "Shock Waves and Reaction-Diffusion Equations," Springer-Verlag, New York, 1983, pp. 346–367.

[2]Chang, T., and Hsiao, L., "The Riemann Problem and Interaction of Waves in Gas Dynamics," *Pitman Monographs and Surveys in Pure and Applied Mathematics,* Longman UK, Wiley, New York, 1989.

[3]Godunov, S. K. (ed.), *Numerical Solution of Multi-Dimensional Problems in Gas dynamics,* Nauka Press, Moscow, Russia, 1976, Chap. 2.

[4]Roe, P. L., "Approximate Riemann Solvers, Parameter Vectors and Difference Schemes," *Journal of Computational Physics,* Vol. 43, No. 2, 1981, pp. 357–372.

[5]Toro, E. F., "A Linearised Riemann Solver for the Time-Dependent Euler Equations of Gas Dynamics," *Proceedings of the Royal Society of London,* Series A, Vol. 434, 1991, pp. 683–693.

[6]Harten, A., Lax, P. D., and Van Leer, B., "On Upstream Differencing and Godunov-Type Methods," *SIAM Review,* Vol. 25, No. 1, 1983, pp. 35–61.

[7]Toro, E. F., Spruce, M., and Speares, W., "Restoration of the Contact Surface in the HLL Riemann Solver," Cranfield Inst. of Technology, Rept. CoA-9204, Bedfordshire, England, UK, Jan. 1992.

[8]Gottlieb, J. J., and Groth, C. P. T., "Assessment of Riemann Solvers for One-Dimensional Inviscid Flows for Perfect Gases," *Journal of Computational Physics,* Vol. 78, No. 2, 1988, pp. 437–458.

[9]Glimm, J., "Solutions in the Large for Nonlinear Hyperbolic Systems of Equations," *Communication in Pure and Applied Mathematics,* Vol. 18, 1965, pp. 697–715.

[10]Roe, P. L., and Pike, J., "Efficient Construction and Utilisation of Approximate Riemann Solutions," *Computing Methods in Applied Science and Engineering,* edited by R. Glowinski and J. L. Lions, Vol. VI, North-Holland, Amsterdam, The Netherlands, 1984, p. 499.

[11]Toro, E. F., "A Fast Riemann Solver with Constant Co-Volume Applied to the Random Choice Method," Cranfield Inst. of Technology, Rept. CoA-8719, Bedfordshire, England, UK, 1987.

[12]Dukowicz, J. K., "A General Non-Iterative Riemann Solver for Godunov's Method," *Journal of Computational Physics,* Vol. 61, 1985, pp. 119–137.